Mode-coupled artifact standard for polarization-mode dispersion: design, assembly, and implementation

Paul A. Williams

A stack of quasi-randomly oriented quartz plates has been assembled as a calibration artifact for mode-coupled polarization-mode dispersion. The design of the artifact, the reasons for choosing it, the procedure for its assembly, and its implementation are described. Considerable discussion is also devoted to the fact that this mode-coupled artifact is limited in scope to polarimetric measurement techniques (those that directly measure differential group delay as a function of wavelength).

OCIS codes: 060.2270, 060.2300.

1. Introduction

The statistical nature of polarization-mode dispersion (PMD) makes it difficult to verify accuracy and precision of mode-coupled PMD measurements. Early attempts at interlaboratory comparisons with spools of single-mode fiber demonstrate that the inherent instability of the mode-coupling sites in fiber make it a poor artifact for calibration of PMD measurement systems.[1,2] We have developed a fixed-mode-coupling artifact (a stack of quartz plates) with a PMD signature similar to that of a single-mode fiber but without the associated environmental instability. We discuss the design details, assembly, environmental stability, and measurement uncertainties of this artifact that was developed as a Standard Reference Material (SRM 2518) by the National Institute of Standards and Technology.

Before beginning the discussion, some definitions should be stated. Differential group delay (DGD) refers to the difference in propagation time between two orthogonally polarized states of light that are launched along the fast and the slow principle states of polarization of the device in question. In mode-coupled devices, the DGD is a wavelength-dependent quantity, and so a measured DGD is associated with a particular wavelength. The terms PMD and DGD are often used interchangeably, but here, we refer to DGD as the instantaneous value (at a fixed time and measurement wavelength) and PMD as the statistical mean of the DGD averaged over wavelength. Thus the following equivalent expressions are used interchangeably: PMD, mean DGD, and $\langle \text{DGD} \rangle_\lambda$. Also, PMD is referred to by use of the historical symbol $\Delta\tau$.

2. Design

The PMD behavior of a mode-coupled fiber can be modeled by a collection of birefringent elements whose axes are not aligned with each other so that, between each element, the polarization eigenmodes of the elements are coupled.[3] We used this model to design the PMD SRM shown in Fig. 1. The device consists of a stack of 33 to 35 quartz plates cemented together with their optic axes intentionally misaligned. The stack is pigtailed with single-mode fiber and connectorized with angled physical contact connectors (wide key). We also considered a design based on multiple splices of polarization-maintaining fiber (PMF), but rejected it for reasons outlined in Appendix A.

If all wave plates were of the same thickness, the DGD would be a periodic function of wavelength with a period equal to $\lambda^2/(c\Delta\tau)$, where λ is the measurement wavelength, c is the speed of light, and $\Delta\tau$ is the PMD of one of the quartz plates. This is the wavelength period with which the retardance of a single plate repeats. At a wavelength of 1525 nm, this is a periodicity of 123 nm for 2.02-mm-thick plates. Since a periodic DGD is not very fiberlike, we replaced five of the plates with thinner, 1.2-mm-thick plates. The ideal would be to have each wave plate be a different thickness. However, this increases the material cost and does not significantly increase the randomness of the measured DGD.

P. A. Williams (paul.williams@nist.gov) is with the Optoelectronics Division, National Institute of Standards and Technology, MS 815.02, 325 Broadway, Boulder, Colorado 80303-3328.
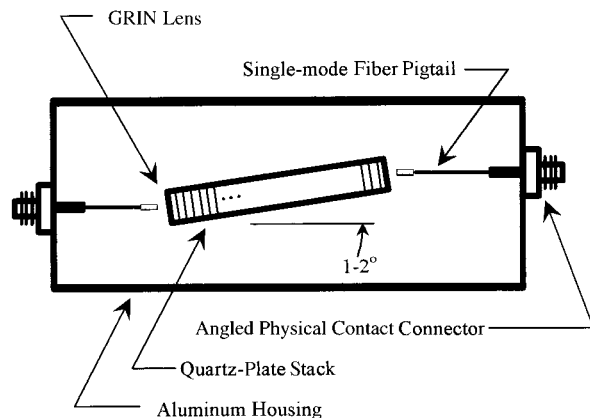
Fig. 1. Diagram of mode-coupled artifact (SRM 2518). Wave-plate stack is tilted by 1–2° with respect to the incident light to prohibit the capture of double-reflected light by the collection GRIN lens.

Fig. 2. DGD versus wavelength curves (a) for a 25-km spool of single-mode fiber and (b) for a quartz plate stack of 35 plates.

In choosing the number, thickness, and orientation of the quartz plates, we were constrained by the need for random mode coupling with low insertion loss and low assembly cost. More wave plates in the stack give a more random mode coupling, but the longer stack has a higher insertion loss. This is due to the inability to collimate light over long distances and then to couple it efficiently into single-mode fiber. We determined when the mode coupling was random enough by computer simulation of the PMD for a given arrangement of wave plates in the stack. We chose the wave-plate arrangement that produced a DGD with a wavelength behavior similar to that of a typical single-mode fiber, that is, a curve that was not flat with wavelength but had features of significant size. Although this test is somewhat subjective, it is sufficient. After all, the goal in using the SRM is that it is a stable artifact whose PMD resembles that of a typical single-mode fiber. This fiberlike DGD behavior is illustrated in Fig. 2, which shows DGD-versus-wavelength curves from a 25-km long section of single-mode fiber and from the 35-plate stack. The stack shows the quasi-random DGD-versus-wavelength behavior expected of a mode-coupled fiber.

The selected design geometry is listed in Table 1 (list of plate thickness and orientation angle). Initially, we had hoped that building the stacks according to a prescribed map would allow us to predict theoretically the exact DGD-versus-wavelength signature of the SRM. However, after assembling a few stacks, we concluded that the uncertainties of the assembly [wave-plate orientation ±0.5°, birefringence in the graded-index (GRIN) lenses, fiber birefringence, and pigtailing alignment errors] were enough that the output DGD could not be well predicted. Figures 3(a) and 3(b) show theoretical and experimental values of DGD versus wavelength for a 12- and a 35-plate stack, respectively. The qualitative agreement is good but insufficient for an accurate t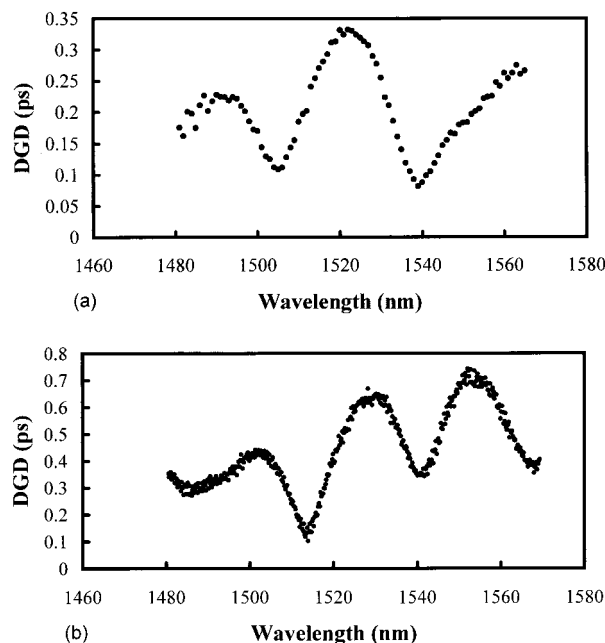heoretical prediction of DGD. So, we still assemble the SRM's according to the map of Table 1, but their performances are not expected to match the theoretical prediction. In fact, difficulties in the manufacturing process caused some of the SRM's to end up with less than 35 plates (33 or 34). So each SRM has its own characteristic PMD behavior and had to be certified separately.

3. Assembly

The SRM's are assembled in three steps. First the stack of quartz plates is assembled, then three cores are drilled from the stack (yielding three identical stacks), and finally the cores are pigtailed and packaged. The assembly began with 1-in. (25.4-mm-) diameter quartz plates. These blanks came standard with a 2.02 ± 0.02-mm thickness. For each stack, 5 of the 35 plates were polished to 1.16 ± 0.01 mm. The fast axis of each plate was identified, and the plates were cemented together so that the angles between the fast axes correspond to Table 1. Figure 4 illustrates the assembly process. An ultraviolet-light-cured index-matching cement was used to hold the plates together.[4] A good index match is important for reducing reflections from within the stack. For polarimetric measurements of PMD, multiple reflections do not bias the measured result, but appear as noise, which averages to 0 with variation of temperature or wavelength.[5]

Once the 35-plate stack was completed, it was sent to a second vendor who drilled three 8.8-mm-diameter cores per stack as shown in Fig. 5. This was done to triple the yield of the stack. This process means that, though each stack is unavoidably built with a slightly different geometry, it yields three SRM's with almost identical PMD characteristics. The core drilling has a few pitfalls. Often one face of

Table 1. Assembly List for Stack of 35 Quartz Plates

Plate #	d^a (mm)	$R(°)^b$
1	2.0	0
2	2.0	−9
3	2.0	88
4	1.2	114
5	2.0	19
6	2.0	74
7	2.0	7
8	1.2	82
9	2.0	86
10	2.0	6
11	1.2	31
12	2.0	51
13	1.2	103
14	2.0	52
15	2.0	12
16	2.0	−18
17	2.0	15
18	2.0	−21
19	2.0	26
20	2.0	59
21	2.0	9
22	2.0	96
23	2.0	−33
24	2.0	123
25	2.0	26
26	1.2	0
27	2.0	69
28	2.0	62
29	2.0	55
30	2.0	58
31	2.0	50
32	2.0	62
33	2.0	92
34	2.0	63
35	2.0	90

^{a}Thickness of the plate.
^{b}Rotation angle of the fast axis (see Fig. 4 for assembly orientation).

the stack ends up having some chipping around the edge of the core. We did not determine if this was the entrance or the exit face of the core drill. We attempted to correct the problem by waxing glass blanks to the outer faces before drilling and then removing them after. However, it appears that the wax softened during the drilling process, and the glass blank jammed in the core drill, which resulted in one or two of the quartz plates being broken off the end(s) of the stack. We no longer use the protective glass blanks, but instead simply bevel the edges of the core-drilled stacks to remove any chips.

The third step is to package the stacks. Each stack is pigtailed, connectorized, and placed in an aluminum housing (Fig. 1). A low-return-loss pigtail design (Fig. 6) is used to connect the input fiber to the GRIN lens. The stack is also tilted (Fig. 1) so that light enters at an angle (with an air gap between the GRIN lens and the quartz stack) so as to reduce the amount of multiply reflected light that is transmitted. The issue of multiple reflections is dis-
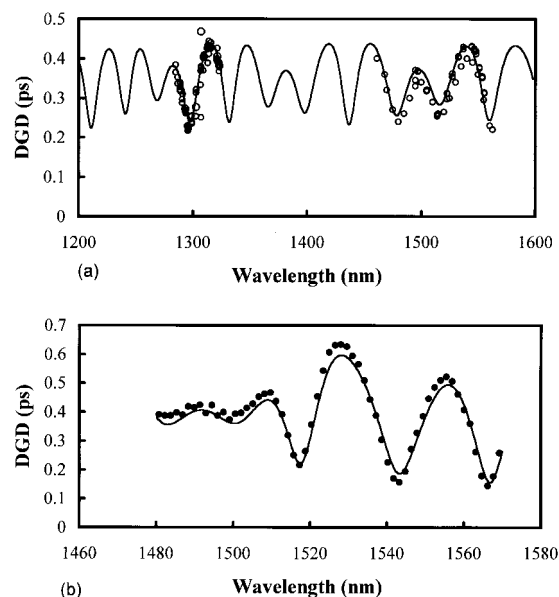

Fig. 3. Agreement between theoretical (curve) and experimental (circles) DGD values as a function of wavelength (a) for a 12-plate stack of quartz plates and (b) for a 35-plate stack of quartz plates.

cussed in more depth in Ref. 3. The basic goal in the design is to prevent any reflected light from passing through the device more than once [multiple reflections in a cavity that does not contain the device under test do not bias the results with a Jones matrix eigenanalysis (JME) measurement, which is the technique we use to certify the artifacts].

A schematic of the launch and receive geometry is shown in Fig. 7, where I_0, I_1, and I_2 denote the incident, transmitted, and forward-reflected beams.
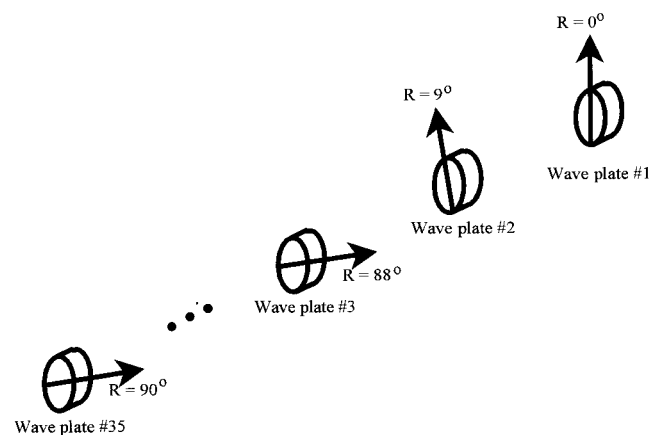

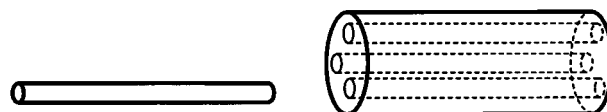Fig. 4. Schematic of wave-plate assembly orientations according to Table 1. The arrow indicates the fast axis.

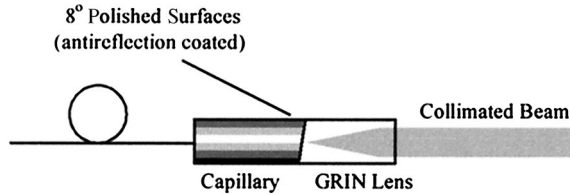Fig. 5. Quartz-plate stacks are core drilled to triple the yield.

Fig. 6. Detail of low-reflection pigtail geometry. The fiber is held in a angle-polished capillary that is cemented to an angled GRIN lens.

The scale (and angles) are exaggerated to illustrate how I_2 is shifted by a distance ρ with respect to I_1 and therefore experiences a much lower coupling efficiency than the primary transmitted beam. The fraction of forward-reflected light that is collected by the output GRIN lens is given by

$$T = \frac{I_2}{I_0} = R_1 R_2 \exp\left(-\frac{2\rho^2}{w^2}\right), \qquad (1)$$

where w is the beam waist, R_1 and R_2 are the intensity reflection coefficients for the first and second reflection surfaces, and the transverse separation between the transmitted and the forward-reflected beams is

$$\rho = \frac{2d\,\cos(\theta)\sin(\theta)}{[n^2 - \sin^2(\theta)]^{1/2}}, \qquad (2)$$

where d is the distance between the two reflections, θ is the tilt angle of the incident light, and n is the index of refraction of quartz. Equation (1) is essentially an overlap integral between two Gaussian functions and gives the ratio of multiply reflected light that is captured by the output GRIN lens divided by the total input power. We assembled the stack with a 1–2° tilt. For the strongest reflections (off the endfaces of the ~66-mm-long stack), we find $T = -75$ dB. Therefore we expect multiple reflections within the stack not to be a problem for this design.

The fiber pigtails are approximately 4 cm long and are single-mode fiber. The ends are terminated with angled physical contact connectors. The angled connector was chosen to minimize reflections passing through the device. The device was held in an aluminum housing with bulkhead adapters for making
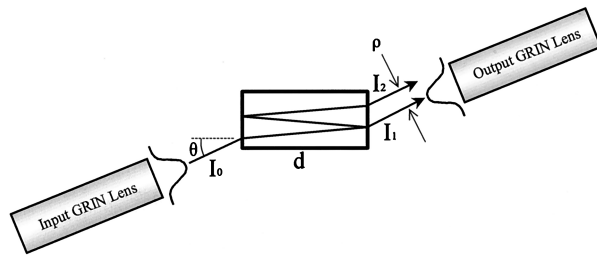

Fig. 7. Schematic of light paths through a quartz-plate stack (not drawn to scale). For a tilt of θ, the transmitted and forward-reflected beams are separated by ρ.

the connection to the device. These female bulkheads have a wide key (N-type).

4. Environmental Stability

As mentioned, the effort to develop a mode-coupled PMD artifact came from the unusually large environmental instability of PMD measurements on spools of single-mode fiber. Large disagreements have been seen for independent (round robin) measurements on spools of single-mode fiber.[1,2] However, it was not possible to determine how much disagreement was due to differences between the participants' measurement systems and how much was merely the statistical uncertainty inherent in long mode-coupled fibers. Indeed, Poole and Favin[3] predict this inherent uncertainty to be 23% for a fiber with 0.3 ps of PMD measured with a 100-nm source. This large statistical variation comes from changes in locations of mode-coupling sites along the length of the fiber. These sites are usually due to microbends of the fiber or some other defects and generally change as the fiber is moved or the temperature is changed.

Since environmental instability motivated the search for a more suitable transfer artifact for mode-coupled PMD, it is appropriate to discuss the environmental stability of the quartz-plate stack. In this discussion, an understanding of the difference between phase birefringence Δn and group birefringence Δn_g is necessary. Appendix B offers a quick comparison. Temperature affects the quartz plates in the stack by changing their birefringence and their physical length L. This change affects the DGD in two ways. First, the magnitude of DGD at each wavelength is proportional to $\Delta n_g L$. This temperature dependence could be estimated with the normalized quantity

$$\gamma_g = (l/\Delta n_g L)\mathrm{d}(\Delta n_g L)/\mathrm{d}T.$$

However, we found no measurements of γ_g of quartz in the literature, so instead, we made the assumption that

$$\gamma_g \approx \gamma = (1/\Delta n L)\mathrm{d}(\Delta n L)/\mathrm{d}T.$$

For quartz, $\gamma = -1.232 \times 10^{-4}/°C$ at 1535.59 nm.[6] For the wave-plate stacks used in the SRM's, the nominal mean DGD is 0.5 ps. So we predict this first source of temperature dependence to be of the order of $\alpha_g = \gamma \Delta n L/c = -0.06$ fs/°C.

However, there is a second, more complicated contribution to the temperature dependence of the SRM that is due to the temperature dependence of the retardance γ (not γ_g) and results in a wavelength-dependent shift of DGD(λ). The shape of the DGD(λ) curve is determined by the retardance between each wave plate and the relative orientations of the plates. The retardance δ of a single wave plate is given by the expression

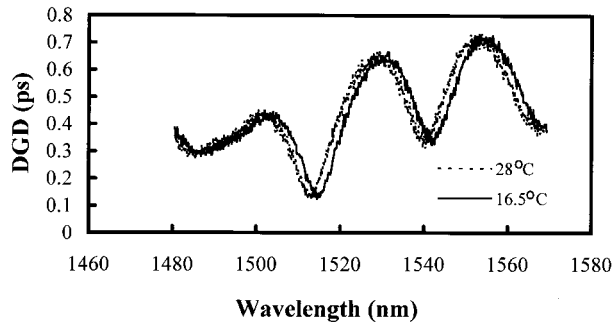$$\delta = 2\pi\left(\frac{\Delta n L}{\lambda}\right). \qquad (3)$$

Fig. 8. Experimental demonstration of wavelength shift for the fixed-mode-coupling stack of 35 plates measured at 16.5 °C and 28 °C.

Clearly, a change in ΔnL is indistinguishable from a change in λ. Therefore, a temperature-induced change in ΔnL effectively shifts the DGD(λ) curve in wavelength. Figure 8 shows an example of two DGD-versus-wavelength curves for the same waveplate stack measured at different temperatures. When the mean DGD is measured at two different temperatures, it is the equivalent of measuring the same curve over two slightly different wavelength ranges. The magnitude of this temperature dependence depends on two factors: the temperature dependence of this effective wavelength shift $d\lambda'/dT$ and the wavelength dependence of the mean DGD,

$$\frac{d\langle DGD \rangle_{\lambda'}}{d\lambda'} \equiv \frac{\dfrac{d}{d\lambda'}\left(\displaystyle\int_{\lambda_1+\lambda'}^{\lambda_2+\lambda'} DGD(\lambda)d\lambda\right)}{\lambda_2 - \lambda_1}. \qquad (4)$$

The quantity in Eq. (4) is merely the derivative of the mean DGD with respect to the starting wavelength over which it is averaged. The temperature dependence of the mean DGD due to this wavelength shift can then be expressed as

$$\alpha_p = \frac{d\langle DGD \rangle_{\lambda'}}{d\lambda'} \frac{d\lambda'}{dT}. \qquad (5)$$

Therefore, the total temperature dependence of the mean DGD can be estimated as

$$\alpha = \alpha_g + \alpha_p = \frac{d\langle DGD \rangle_{\lambda'}}{d\lambda'} \frac{d\lambda'}{dT} + \frac{\gamma \Delta nL}{c}. \qquad (6)$$

The quantity $d\langle DGD \rangle_{\lambda'}/d\lambda'$ depends on the exact shape of the DGD-versus-wavelength curve and cannot be estimated. We directly measured $\langle DGD \rangle_{\lambda'}/d\lambda'$ for each wave-plate stack and over each wavelength range of interest.

We estimate the strength of $d\lambda'/dT$ by equating the wavelength dependence of the retardance

$$\frac{d\delta}{d\lambda} = 2\pi \Delta nL\left(-\frac{1}{\lambda^2}\right), \qquad (7)$$

with the temperature dependence of the retardance

$$\frac{d\delta}{dT} = \frac{2\pi}{\lambda} \frac{d(\Delta nL)}{dT}. \qquad (8)$$

We find

$$\frac{d\lambda'}{dT} = \frac{d\delta}{dT} \bigg/ \frac{d\delta}{d\lambda} = -\gamma\lambda. \qquad (9)$$

Using the temperature dependence of quartz,

$$d\lambda'/dT = -\lambda\gamma = 0.19 \text{ nm/°C}$$

at 1536 nm. Unfortunately, quartz is not the only component contributing to this wavelength shift. Temperature-dependent wavelength shifts could come from birefringences in the GRIN lenses, the cement between the quartz plates, or any stress birefringence in the plates themselves. Although these factors do not contribute significantly to the average DGD of the device, they could easily contribute to the temperature-dependent wavelength shift of the DGD(λ) profile of the SRM. We measure the temperature-dependent wavelength shift individually for each SRM. We do this by measuring DGD(λ) curves at 23 °C and 26 °C. This yields two DGD-versus-wavelength curves slightly shifted in wavelength with respect to each other (Fig. 8). The two DGD(λ) curves are cross correlated to yield the wavelength shift due to the 3 °C temperature change. On the various SRM's tested, we measured values of $d\lambda'/dT$ between -0.1 and -0.18 nm/°C, which is reasonably close to the theoretical estimate -0.19 nm/°C. In performing the uncertainty analysis on the SRM's, we used a conservative estimate of $d\lambda'/dT = -0.3$ nm/°C (which is larger than any of our measured values) for all of the SRM's. We then tested these estimated uncertainties due to temperature by comparing measurements of mean DGD made at 23 °C to identical measurements made at 26 °C and by verifying their equivalence to within the uncertainty.

5. Measurement Uncertainty and Device Certification

Uncertainties associated with the measurement of the PMD of the wave-plate stack come from two sources: the environmental instability of the stack being measured and the inaccuracies of the measurement system. The environmental instability of the wave-plate stack is due only to temperature. This dependence is included in the uncertainty statement as $\alpha\Delta T$, where α is the temperature dependence from Eq. (6) and ΔT represents the temperature range over which the device is certified. As mentioned, PMD is sensitive to the wavelength range of the measurement. This uncertainty is expressed as $\Delta\lambda(d\langle DGD \rangle_{\lambda'}/d\lambda')$, where $\Delta\lambda$ is the allowed uncertainty of the start and the stop wavelengths for the DGD averaging. We certified the PMD of the stacks using a rotating-wave-plate polarimeter[5] to perform a JME measurement,[7] which yields the DGD versus wavelength for the

device being tested. The standard uncertainty of our polarimeter is documented in Ref. 5 and is denoted here as σ_{JME}.

The remaining uncertainty comes from the random uncertainty of the measurement. This is, essentially, the standard deviation of multiple measurements. The certified value of PMD for each wave-plate stack was the result of several wavelength scans, all contained within the range of 1480 to 1570 nm. To eliminate systematic errors due to multiple reflections[5] within the SRM or the measurement system, each full scan of DGD versus wavelength consisted of five separate runs in which DGD data was sampled in 1-nm steps over the 90-nm range (yielding 89 points). Each of the five runs had a starting wavelength that was 0.2 nm larger than the previous run. The result of the five runs was a DGD-versus-wavelength table containing 445 points spaced in 0.2-nm steps starting at 1480.5 nm and ending with 1569.3 nm. At least two sets of DGD scans (five runs each) were performed with the fiber leads between the measurement system and the SRM reoriented between scans. We calculated the weighted mean standard deviation σ_ε of each DGD value as a function of wavelength by locally detrending the data.[8] The standard deviation between the means of each 445-point scan was also calculated and is denoted σ_S. The random uncertainty of the measurement is then reported according to the variance-component model[9] as

$$\sigma_R = \left(\frac{\sigma_S{}^2}{N_S} + \frac{\sigma_\varepsilon{}^2}{N_{\mathrm{Tot}}}\right), \qquad (10)$$

where N_S is the number of scans (a small number greater than 2), and N_{Tot} is the total number of data points measured.

The total (expanded) uncertainty of the certification measurements is given by

$$2u_{\mathrm{Tot}} = 2\left\{\sigma_{\mathrm{JME}}{}^2 + (\alpha\Delta T)^2 + \left[\frac{\sigma_S{}^2}{N_S} + \frac{\sigma_\varepsilon{}^2}{N_{\mathrm{Tot}}}\right] + \left(\Delta\lambda\,\frac{\mathrm{d}\langle\mathrm{DGD}\rangle_{\lambda'}}{\mathrm{d}\lambda'}\right)^2\right\}^{1/2}. \qquad (11)$$

The factor of 2 is a coverage factor representing an approximate 95% confidence interval. This uncertainty is generally dominated by the uncertainty of the measurement system, $\sigma_{\mathrm{JME}} = 1.6$ fs for our measurement system.[5]

We certify the SRM's over 25 different wavelength ranges (all contained within the 90-nm scan range of our tunable laser). For each scan range, we report an uncertainty based on Eq. (11). The value ΔT represents the temperature uncertainty that is allowed in the certification. Two uncertainty values are reported: one for 23 ± 1 °C and one for 23 ± 3 °C. This is done to allow use of the SRM for different levels of temperature control. A $\Delta\lambda = \pm0.2$-nm wavelength uncertainty is allowed and is taken into account in the last term of Eq. (11).

6. Scope of Use for Certified Wave-Plate Stack Standard Reference Material

The certified values of PMD quoted for this artifact apply only to measurements of PMD made by use of polarimetric techniques. The term polarimetric is used here to denote PMD measurement techniques that directly measure DGD as a function of wavelength. Polarimetric techniques include JME,[7] Poincaré arc [also called state of polarization[10] (SOP)] and modulation phase shift.[11] Other techniques not mentioned here that directly measure DGD versus wavelength should also be certifiable with this SRM. Nonpolarimetric measurement techniques such as fixed analyzer with extremum counting (FAEC), fixed analyzer with Fourier transform analysis (FAFT), and low-coherence interferometry (INT) are not certified with this technique.

Because of the popularity and usefulness of nonpolarimetric techniques, it is worthwhile to spend some time explaining the details that require this limitation in scope. First, this limitation in scope is in no way a judgement of the performance or validity of any of these measurement techniques. This limitation merely acknowledges that polarimetric techniques are well suited to calibration by a fixed-mode-coupling artifact and that nonpolarimetric techniques are not.

To understand this, it is useful to illustrate the differences between PMD measurements on a real fiber (variable, random mode coupling) and on a wave-plate stack (fixed, random mode coupling). The DGD in a highly mode-coupled, single-mode fiber varies in a quasi-random manner as a function of wavelength. The statistical behavior of DGD follows a maxwellian distribution whose expected value $\langle\Delta\tau\rangle$ is a function of the intrinsic birefringence of the fiber and is independent of the location of the mode-coupling sites. Therefore it is generally accepted that there are two equivalent methods of characterizing a fiber's DGD statistics. Either the fiber can be held in a fixed position with multiple DGD measurements made over various nonoverlapping wavelength ranges, or multiple DGD measurements can be made at a single wavelength while the mode-coupling geometry of the fiber is changed (by one's either moving the fiber or changing its temperature).[12] This equivalence requires the assumption of a highly mode-coupled fiber with stationary PMD. In practice, the best estimates of the mean DGD of a fiber come from a combination of both methods.

If two experimenters want to compare PMD measurements on the same piece of fiber, they are attempting to measure the expectation value of DGD. We denote this true mean (expected value) of DGD as $\langle\Delta\tau\rangle$ and the measured mean as $\Delta\tau$. In practice, one can estimate $\langle\Delta\tau\rangle$ by measuring $\Delta\tau$ over a finite wavelength range. The uncertainty of the estimate depends on the size of the wavelength range and on $\langle\Delta\tau\rangle$ itself. Gisin *et al.*[13] have demonstrated experimentally an approximate equivalence between the statistical uncertainties of the various PMD measurement
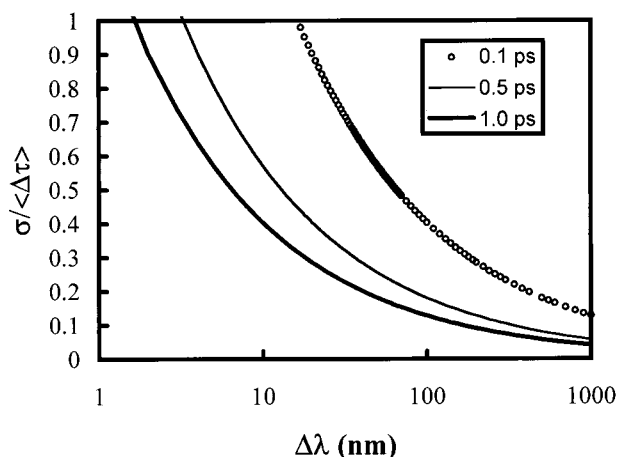
Fig. 9. Estimated fractional uncertainty versus measurement bandwidth for various PMD values obtained with Eq. (12).

techniques. Assuming this equivalence, we use the uncertainty derived by Poole and Favin[3] for the particular case of FAEC measurements and apply it to all PMD measurement techniques. The fractional standard deviation of $\Delta\tau$ measured over a frequency range $\Delta\omega$ is

$$\frac{\sigma}{\langle\Delta\tau\rangle} = \left[\frac{0.21(2\pi)}{\langle\Delta\tau\rangle\Delta\omega}\right]^{1/2} = \frac{1.15}{(\langle\Delta\tau\rangle\Delta\omega)^{1/2}}. \quad (12)$$

This fractional uncertainty is plotted as a function of the measurement bandwidth for various PMD values in Fig. 9. This picture illustrates the statistical difficulties in comparing PMD measurements on fiber specimens. For the case of a fiber with $\langle\Delta\tau\rangle = 0.1$ ps, a 100-nm wavelength range (typical of a tunable laser used in JME measurements, or possibly an edge-emitting LED (EELED) from an INT system) would yield a measurement standard deviation of 40%. At this point, an experimenter could change the mode-coupling characteristics of the fiber (through temperature or time) and repeat the measurement to increase the number of statistically independent samples. For a standard uncertainty of 5% to be obtained, 64 statistically independent measurements would have to be made (assuming that N statistically independent measurement scans reduce the standard deviation by $1/N^{1/2}$). For a 1% uncertainty, 1600 independent scans would be needed. In practice, fiber measurements of reasonable uncertainties are difficult to obtain. The situation could be somewhat better for a fixed-analyzer system able to use much broader sources with spectral widths of as much as 500 nm or so. However, even in this case, a single 500-nm scan still yields an 18% uncertainty.

Clearly, a fiber with variable mode-coupling geometry is not well suited to be a transfer standard due to its inherently large measurement uncertainty. We chose, therefore, to use a fixed-mode-coupling device (a mode-coupled stack of wave plates whose location and strength of mode-coupling sites are fixed). This necessitates a change in operation. A fixed-mode-

coupling device cannot be certified for $\langle\Delta\tau\rangle$, but only for $\Delta\tau$. That is, since the mode-coupling geometry cannot be changed, multiple measurements of $\Delta\tau$ over a given wavelength range are not statistically independent. The only statistically independent measurements comes from different wavelength ranges. Using Eq. (12), we see that in a fixed-mode-coupling geometry, an estimate of $\langle\Delta\tau\rangle$ with a 5% uncertainty (for our 0.5-ps artifact) would require the unrealistic wavelength scan range of 1300 nm. Therefore we do not attempt to certify the expectation value of the stack's DGD $\langle\Delta\tau\rangle$, but rather simply use a specific technique to certify the mean DGD $\Delta\tau$ for measurements over a specific wavelength range. In fact, we certify the SRM only for a polarimetric measurement of the mean DGD value $\Delta\tau$ measured over a given wavelength range. We can quote a 1% uncertainty for this value. This value agrees with any polarimetric measurement of mean DGD as long as it is made over the specified wavelength range. And, as mentioned, this value is not an estimator of the mean DGD to be measured by any nonpolarimetric techniques (FAEC, FAFT, or INT).

A given measurement technique measures the average DGD $\Delta\tau_1$ over a given wavelength range $\Delta\omega$. This value $\Delta\tau_1$ is a single number from a statistical ensemble whose mean is $\langle\Delta\tau\rangle$ and whose standard deviation is given by Eq. (12). A different (nonpolarimetric) measurement technique used to measure over the same wavelength range yields an average DGD value $\Delta\tau_2$, which is drawn from the same ensemble as $\Delta\tau_1$. However, it is not expected that $\Delta\tau_1 = \Delta\tau_2$. So, if a fixed-mode-coupling artifact is to be used to demonstrate agreement between various measurement techniques, it can do so only within an uncertainty determined by Eq. (12), i.e., 20–40% for typical wavelength ranges. This accuracy is so severely limited by the finite spectral width of the methods that intermethod comparisons with a fixed-mode-coupling artifact may actually be less useful than comparisons simply with fiber. Indeed, fiber-based comparisons of PMD measurement techniques have yielded results with uncertainties in the 5–10% range.[14–16]

A question arises as to why the SRM is certified only for polarimetric PMD measurements. It turns out to be a matter of uncertainty. Individual characterization of the SRM for each of the nonpolarimetric techniques is not possible to the same uncertainty as with the polarimetric techniques. One problem lies in the inability to control the input SOP owing to birefringence in the fiber leads connecting the measurement system to the test artifact. With polarimetric measurements, this is not an issue, since the absolute orientation of the entrance SOP does not affect the measured DGD. However, with the FAEC technique, for example, the intensity spectrum of a mode-coupled device can change completely if the input SOP is changed slightly. A similar result occurs in INT measurements.

We illustrate this using computer simulation. Figures 10–12 show histograms for simulated FAEC,

FAFT/INT, and JME measurements of $\Delta\tau$ over a 200-nm wavelength range on a 35-quartz-plate stack (fixed mode coupling). Each histogram represents the result of 100 measurements made with the fiber leads rearranged between each measurement. The computer simulation used a random orientation of 35 quartz plates (30 of which are 2 mm thick and 5 that are 1.2 mm thick) as the stack geometry. The orientations of these plates remained fixed throughout the entire simulation. Birefringence in the leads was simulated as two 50-μm-thick quartz plates, one on each end of the stack, whose orientations were randomized before each simulated measurement. Given this geometry, the wavelength-dependent Jones matrices were calculated for the stack at 256 wavelength points evenly spaced over the 200-nm range. From these Jones matrices, the spectral intensity was calculated, assuming that a fixed-analyzer geometry (stack between crossed polarizers) was used. From this spectral intensity and the
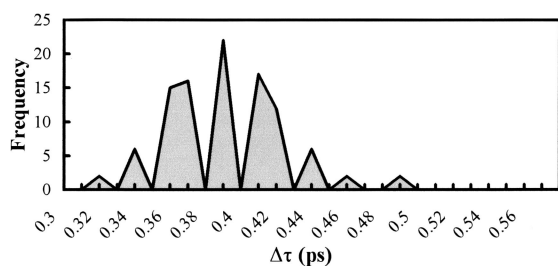

Fig. 10. PMD histogram of 100 FAEC measurements of a 35-plate stack with fiber leads manipulated between each measurement (simulation).
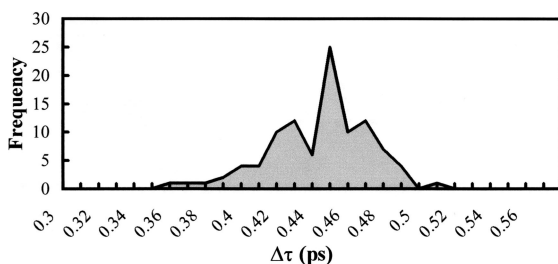

Fig. 11. PMD histogram of 100 FAFT or equivalently interferometric measurements of a 35-plate stack with fiber leads manipulated between each measurement (simulation).
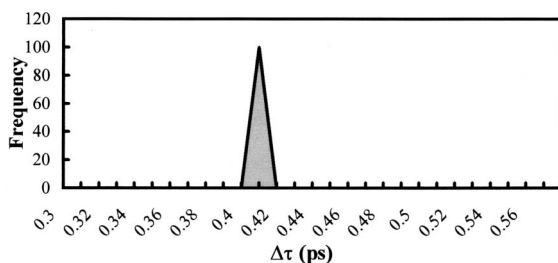

Fig. 12. PMD histogram of 100 JME measurements of a 35-plate stack with fiber leads manipulated between each measurement (simulation).

wavelength-dependent Jones matrices, FAEC, FAFT (or equivalently INT), and JME estimates of PMD were found.

Two observations come from the histograms of Fig. 10–12. First, the figures clearly illustrate our claim that, in a fixed-mode-coupling device, it is not possible to measure the expectation value $\langle\Delta\tau\rangle$. Figures 10–12 represent measurements on the same device over the same 200-nm wavelength range, and yet the mean DGD values measured by each of the techniques do not agree with each other. The mean of the 100 $\Delta\tau$ values measured by FAEC is 0.386 ps, whereas the interferometric measurements gave a mean $\Delta\tau = 0.440$ ps [this value is already converted from rms to mean DGD by the well-known factor of 1.085 (Ref. 17), and the mean DGD from the JME simulation gave $\Delta\tau = 0.406$ ps. Clearly, a fixed-mode-coupling artifact does not yield the same PMD value when measured by different techniques even over identical wavelength ranges. This is as expected.

The second observation from Figures 10–12 is the relative widths of the histograms. Clearly, for JME measurements, reorienting the fiber leads has no significant effect on the measured $\Delta\tau$ value (Fig. 12). However, in the case of FAEC or INT, the lead reorientation allowed a considerable spread in $\Delta\tau$ values (standard deviation $\sigma = 9\%$ for FAEC and 6% for INT as opposed to 0.1% for JME). These uncertainties are complicated by the histograms being non-Gaussian (for example, the FAEC curve has discrete spikes corresponding to discrete numbers of peaks and valleys in the spectrum). Also, the simulations achieved this ensemble of $\Delta\tau$ measurements by reorienting the fiber leads in a truly random way in between each measurement. In practice, this would be difficult to obtain and hard to verify.

The uncertainty in nonpolarimetric measurements of $\Delta\tau$ is further complicated by the fact that users of interferometric techniques cannot control the spectrum of their source. As mentioned, measured values of $\Delta\tau$ in a fixed-mode-coupling artifact depend on the exact wavelength range of measurement. Since interferometers tend to use EELED sources, the wavelength spectrum of the source depends on the particular EELED used. This situation makes it difficult to certify adequately the value of $\Delta\tau$ to be measured with the interferometric technique. It would essentially require an individual calibration for each customer's source EELED. As an experimental example, using one INT system with four different randomly selected EELED sources we measured a prototype fixed-mode-coupling wave-plate stack. The EELED's had center wavelengths ranging from 1538.4 to 1555.3 nm and full width half-maximum (FWHM) values ranging from 52.9 to 101.3 nm. For each source used, 30 measurements of $\Delta\tau$ were made with fiber leads randomly reoriented between each measurement. The four mean $\Delta\tau$ values (each averaged over 30 measurements) disagreed with each other by as much as 13% for the various sources.

These extra uncertainties make calibration of nonpolarimetric measurement techniques with a fixed-mode-coupling artifact impractical. The uncertainty that would have to be assigned to the certified value of the calibration artifact would be too large to make the artifact useful for absolute calibration. However, this SRM design might be useful for the nonpolarimetric techniques simply as a quality-control device that a user could measure periodically with their nonpolarimetric system simply to verify the measurement precision (without a certification on the accuracy). The usefulness of this would rely on multiple measurements to reduce the uncertainties illustrated in Figs. 10 and 11.

7. Conclusions

The mode-coupled artifact described here has demonstrated the necessary environmental stability to provide useful calibration to polarimetric measurement techniques. The question remains as to the best way to calibrate nonpolarimetric techniques. A single birefringent element (quartz plate) is a non-mode-coupled solution. However, there is currently no mode-coupled PMD artifact that could be measured by all the measurement techniques and expected to yield the same result for each.

Appendix A: Alternative Design—Spliced Polarization-Maintaining Fiber

Since PMD can be modeled as a stack of birefringent elements, it is possible to make a PMD emulator from many randomly oriented splices of PMF. However, we chose to use quartz plates because they could yield a PMD that was in the target range of approximately 0.5 ps. We found it difficult to make a section of spliced fibers with the spliced sections much shorter than approximately 10 cm. This means that for a PMF with a beat length of 2 mm, each spliced section would have a PMD of approximately 260 fs. For 35 sections of PMF, therefore, the expected value of PMD for a truly random orientation would be $\Delta\tau N^{1/2} = (260 \text{ fs}) \, 5.9 = 1.5 \text{ ps}$, which is significantly larger than the 0.5-ps goal. However, in the case of quartz, a single 2-mm-thick plate has a PMD of approximately 63 fs (with $\Delta n_g = 0.009403$). Thirty-five randomly oriented quartz plates yield a PMD of approximately 63 fs 5.9 = 0.37 ps, which is closer to our target PMD value.

Appendix B: Significance of Phase and Group Birefringence

When discussing birefringence in the case of PMD, it is important to specify whether this is phase birefringence Δn or a group birefringence Δn_g. The two are related as[18]

$$\Delta n_g = \Delta n - \lambda (\mathrm{d}\Delta n / \mathrm{d}\lambda). \qquad (B1)$$

Figure 13 illustrates the differences in Δn and Δn_g over the wavelength range of interest.[19–21] In practice, the phase birefringence is used in cases in which the relative phases of light traveling in the two po-
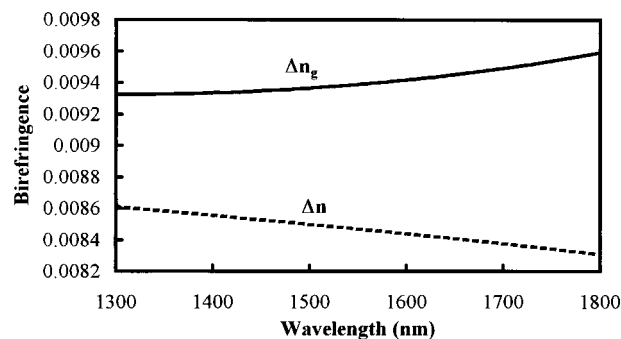

Fig. 13. Wavelength dependence of phase birefringence Δn and group birefringence Δn_g for quartz. The Δn curve is a third-order polynomial fit to the data from Refs. 19–21, and the Δn_g curve was calculated from the Δn curve and Eq. (B1).

larization eigenmodes is the parameter of interest. For example, the retardance δ of a single wave plate (thickness L) depends on the phase birefringence as $\delta = 2\pi\Delta n L/\lambda$. Group birefringence is used when the parameter of interest is the difference in the velocity of energy flow between two polarization eigenstates. For example, the PMD of a single quartz plate comes from the difference in group velocity between the eigenstates, $\text{PMD} = \Delta n_g L/c$.

References and Notes

1. W. B. Gardner and TIA Ad Hoc Group, "Inter-laboratory polarization mode dispersion measurement study," in *Technical Digest of 1994 Symposium on Optical Fiber Measurements*, National Institute of Standards and Technology Special Publication 864 (National Institute of Standards and Technology, Boulder, Colo., 1994), pp. 171–174.
2. P. A. Williams, "TIA round robin for the measurement of PMD," in *Technical Digest of 1996 Symposium on Optical Fiber Measurements*, National Institute of Standards and Technology Special Publication 905 (National Institute of Standards and Technology, Boulder, Colo., 1996), pp. 155–158.
3. C. D. Poole and D. L. Favin, "Polarization-mode dispersion measurements based on transmission spectra through a polarizer," J. Lightwave Technol. **12,** 917–929 (1994).
4. Norland Optical Adhesive 61, which is stipulated by the manufacturer to have a refractive index of 1.56 (wavelength unspecified).
5. P. A. Williams, "Rotating-wave-plate Stokes polarimeter for differential group delay measurements of polarization-mode dispersion," Appl. Opt. **38,** 6508–6515 (1999).
6. A. H. Rose and S. M. Etzel, National Institute of Standards and Technology, Boulder, Colo., 80303 (personal communication).
7. B. L. Heffner, "Automated measurement of polarization mode dispersion using Jones matrix eigenanalysis," Photon. Technol. Lett. **4,** 1066–1069 (1992).
8. That is, for a slowly varying curve, the random standard deviation can be calculated with the deviation of the data from a local mean value. See J. Rice, "Bandwidth choice for nonparametric regression," The Ann. Statist. **12,** 1215–1230 (1984).
9. F. A. Graybill, *Theory and Application of the Linear Model* (Duxbury, North Scituate, Mass., 1976), p. 606.
10. D. Derickson, *Fiber Optic Test and Measurement* (Prentice Hall, N.J., 1998), pp. 511–512.
11. P. A. Williams, A. J. Barlow, C. Mackechnie, and J. B. Schlager, "Narrowband measurements of polarization-mode dispersion using the modulation phase shift technique," in *Technical Digest of 1998 Symposium on Optical Fiber Mea-*

surements, National Institute of Standards and Technology Special Publication 930 (National Institute of Standards and Technology, Boulder, Colo., 1998), pp. 23–26.

12. N. Gisin, "Solutions of the dynamical equation for polarization dispersion," Opt. Commun. **86,** 371–373 (1991).

13. N. Gisin, B. Gisin, J. P. Von der Weid, and R. Passy, "How accurately can one measure a statistical quantity like polarization-mode dispersion?" IEEE Photonics Technol. Lett. **8,** 1671–1673 (1996).

14. A. J. Barlow and P. A. Williams, SC86, WG1, September 1997 (Edinburgh). A summary of fiber measurements from various sources compiled in a contribution to the International Electrotechnical Commission (IEC). Copies can be obtained from the authors.

15. P. A. Williams, "Accuracy issues in comparisons of time- and frequency-domain polarization mode dispersion measurements," in *Technical Digest of 1996 Symposium on Optical Fiber Measurements*, National Institute of Standards and Technology Special Publication 905 (National Institute of Standards and Technology, Boulder, Colo., 1996), pp. 125–129.

16. P. A. Williams and P. R. Hernday, "Anomalous relation between time and frequency domain PMD measurements," in the *Third Optical Fibre Measurement Conference* (Liège, Belgium, 1995), p. I.2.

17. The factor is derived (but is missing a square-root sign) in Eq. (3) of N. Gisin, R. Passy, J. C. Bishoff, and B. Perny, "Experimental investigations of the statistical properties of polarization mode dispersion in single mode fibers," IEEE Photon. Technol. Lett. **5,** 819–821 (1993).

18. J. D. Jackson, *Classical Electrodynamics* (Wiley, New York, 1975), pp. 299–303.

19. J. H. Shields and J. W. Ellis, "Dispersion of birefringence of quartz in the near infrared," J. Opt. Soc. Am. **46,** 263–265 (1956).

20. W. L. Wolfe and G. J. Zissis, eds., *The Infrared Handbook* (Environmental Research Institute of Michigan, Ann Arbor, 1985), pp. 7–57.

21. B. L. Heffner, "Attosecond-resolution measurement of polarization mode dispersion in short sections of optical fiber," Opt. Lett. **18,** 2102–2104 (1993).